Received: 17 September 2020 | Revised: 13 February 2021 | Accepted: 15 February 2021

DOI: 10.1002/mrm.28765

NOTE

Magnetic Resonance in Medicine

Artifact reduction in free-breathing, free-running myocardial perfusion imaging with interleaved non-selective RF excitations

Hassan Haji-Valizadeh[1] | **Rui Guo**[1] | **Selcuk Kucukseymen**[1] | **Xiaoying Cai**[1,2] | **Jennifer Rodriguez**[1] | **Patrick Pierce**[1] | **Beth Goddu**[1] | **Warren Manning**[1,3] | **Reza Nezafat**[1]

[1]Department of Medicine (Cardiovascular Division), Beth Israel Deaconess Medical Center and Harvard Medical School, Boston, Massachusetts, USA

[2]Siemens Medical Solutions Inc., Boston, Massachusetts, USA

[3]Department of Radiology, Beth Israel Deaconess Medical Center and Harvard Medical School, Boston, Massachusetts, USA

Correspondence
Reza Nezafat, Department of Medicine (Cardiovascular Division), Beth Israel Deaconess Medical Center, 330 Brookline Ave, Boston, MA 02215, USA.
Email: rnezafat@bidmc.harvard.edu

Funding information
Dr. Nezafat is funding by the NIH (5R01HL127015-02, 1R01HL129157-01A1, 5R01HL129185, and 1R01HL154744) and the American Heart Association (15EIA22710040). Dr. Haji-Valizadeh is supported by the NIH (5T32HL007374-41)

Purpose: To reduce inflow and motion artifacts in free-breathing, free-running, steady-state spoiled gradient echo T_1-weighted (SPGR) myocardial perfusion imaging.

Method: Unsaturated spins from inflowing blood or out-of-plane motion cause flashing artifacts in free-running SPGR myocardial perfusion. During free-running SPGR, 1 non-selective RF excitation was added after every 3 slice-selective RF excitations to suppress inflow artifacts by forcing magnetization in neighboring regions to steady-state. Bloch simulations and phantom experiments were performed to evaluate the impact of the flip angle and non-selective RF frequency on inflowing spins and tissue contrast. Free-running perfusion with ($n = 11$) interleaved non-selective RF or without ($n = 11$) were studied in 22 subjects (age = 60.2 ± 14.3 years, 11 male). Perfusion images were graded on a 5-point Likert scale for conspicuity of wall enhancement, inflow/motion artifact, and streaking artifact and compared using Wilcoxon sum-rank testing.

Result: Numeric simulation showed that 1 non-selective RF excitation applied after every 3 slice-selective RF excitations produced superior out-of-plane signal suppression compared to 1 non-selective RF excitation applied after every 6 or 9 slice-selective RF excitations. In vitro experiments showed that a 30° flip angle produced near-optimal myocardial contrast. In vivo experiments demonstrated that the addition of interleaved non-selective RF significantly ($P < .01$) improved conspicuity of wall enhancement (mean score = 4.4 vs. 3.2) and reduced inflow/motion (mean score = 4.5 vs. 2.5) and streaking (mean score = 3.9 vs. 2.4) artifacts.

Conclusion: Non-selective RF excitations interleaved between slice-selective excitations can reduce image artifacts in free-breathing, ungated perfusion images. Further studies are warranted to assess the diagnostic accuracy of the proposed solution for evaluating myocardial ischemia.

KEYWORDS
free-running SPGR, GROG-GRASP reconstruction, ungated free-breathing myocardial perfusion

1 | INTRODUCTION

Myocardial perfusion imaging using cardiovascular magnetic resonance (CMR) can provide a non-invasive assessment of coronary artery disease (CAD) during rest and stress.[1-4] In the Clinical Evaluation of Magnetic Resonance Imaging in Coronary Heart Disease (CE-MARC I)[5] trial, CMR-based myocardial perfusion showed higher sensitivity than single photon emission computed tomography (SPECT) at detecting CAD.[5] In a recent randomized trial, CMR-based myocardial perfusion was shown to be non-inferior to invasive fractional flow reserve (FFR) at predicting major adverse events in patients with typical angina and 2 or more cardiac risk factors.[6] These studies suggest that (1) CMR exhibits high sensitivity and specificity compared to FFR for CAD detection; (2) CMR is superior to SPECT for non-invasive assessment of CAD; and (3) CMR may be non-inferior to FFR at predicting major adverse events.

CMR-based myocardial perfusion imaging is usually performed using electrocardiogram (ECG) triggered acquisition with or without breath-holding. In conventional myocardial perfusion, single-shot images are collected after a short delay with a saturation pulse.[7] Alternatively, several new studies have investigated free-running myocardial perfusion imaging without a saturation pulse. These studies typically involve radial k-space sampling with golden-angle ordering[8] and spoiled steady-state gradient echo (SPGR)-based T_1-weighted acquisition.[9-11] This approach is advantageous compared to conventional myocardial perfusion with saturation pulse because neither ECG-gating nor breath-holding are necessary to produce diastolic and systolic myocardial perfusion imaging.[9,10,12] Additionally, free-running SPGR can be combined with simultaneous multi-slice acquisition (SMS) to enable whole-heart myocardial perfusion imaging.[12,13] However, the image quality of free-running perfusion imaging remains inferior to conventional myocardial perfusion imaging because of through-plane motion and the presence of "flashing" artifacts associated with the inflow of unsaturated blood spins.[9,13] Therefore, there is an unmet need to improve the image quality of free-running myocardial perfusion.

Several strategies have been proposed to suppress image artifacts during free-running SPGR. Tian et al[13] proposed acquiring SPGR with SMS. This strategy enabled multi-slice myocardial perfusion imaging in which inner slices maintained steady-state magnetization regardless of myocardial motion. However, the approach by Tian et al[13] was limited by motion sensitivity in the outer slices and its inability to suppress inflow artifacts from unsaturated blood. Judd et al[14] proposed using a train of non-selective RF excitation to prepare magnetization before segmented SPGR readout. This strategy suppressed inflow and motion artifacts by driving the imaging volume's magnetization to steady-state, but did not allow for ungated, free-breathing perfusion imaging. Sharif et al[15] suggested a hybrid 2D/3D steady-state acquisition scheme to drive the magnetization to steady-state during 2D multi-slice SPGR. This strategy also has the potential to suppress inflow and motion artifacts but has yet to be evaluated during free-breathing.

The purpose of this study was to reduce inflow and motion artifacts in SPGR-based free-running myocardial perfusion imaging. An interleaved non-selective RF excitation was placed after every 3 slice-selective RF excitations of the imaging sequence to suppress motion and inflow artifacts during free-breathing, free-running myocardial perfusion. Bloch simulations and phantom experiments were performed to study the impact of the flip angle and non-selective RF pulse frequency on artifact suppression and tissue contrast. Subsequently, the efficacy of the proposed method at reducing imaging artifacts was assessed in a pilot patient study.

2 | METHODS

2.1 | SPGR with interleaved non-selective RF excitations

Ungated free-running myocardial perfusion sequence is typically acquired with continuous radial k-space acquisition with golden angle ordering (111.25°)[10] (Figure 1A). In this sequence, the inflow of unsaturated magnetization spins causes flashing artifacts, which can impact diagnostic accuracy and overall image quality. To minimize this effect, the sequence was modified as proposed by Sharif et al[15] by interleaving non-selective RF excitations in between continuous slice-selective RF excitations (Figure 1B). The non-selective RF pulses reduce steady-state magnetization sensitivity to cardiac or respiratory motion by exciting both out-of-plane and in-plane magnetic moments. The excitation of in- and out-of-plane moments suppresses inflow artifacts by driving the entire imaging volume (including out-of-plane unsaturated blood and myocardium) to steady-state during continuous imaging.

2.2 | Bloch simulation: out-of-plane signal suppression

Bloch simulation was performed to assess the effect of the non-selective RF excitation flip angle and frequency on the longitudinal magnetization of out-of-plane moments. The following expression was used to calculate steady-state magnetization for out-of-plane moments:

$$M_z(i) = M_0\left(1 - e^{\frac{-TR}{T1}}\right) / \left(1 - \cos(\theta)\, e^{\frac{-TR}{T1}}\right). \quad (1)$$

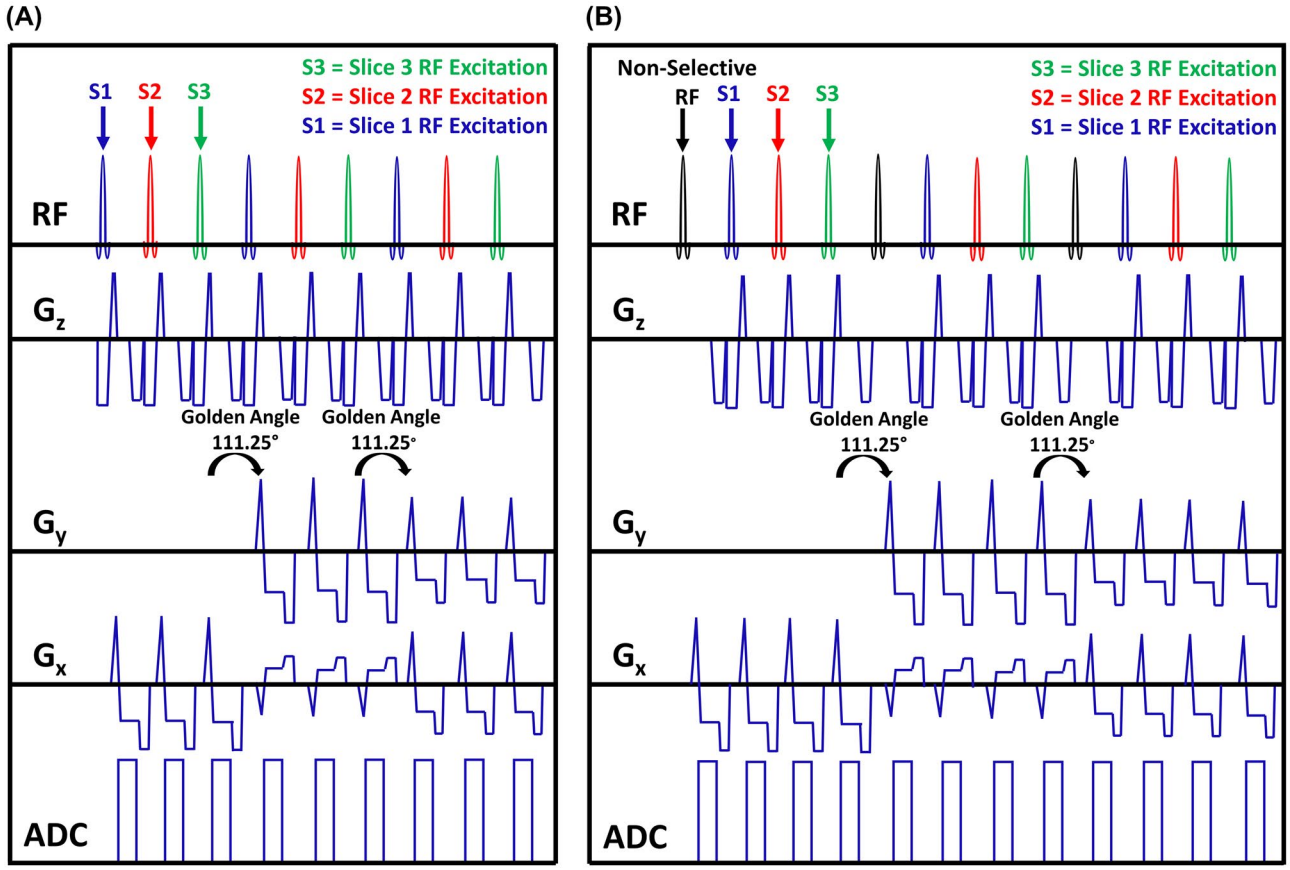

FIGURE 1 Free-running multi-slice myocardial perfusion imaging sequence without (A) and with (B) addition of a non-selective RF excitation pulses. RF, radio-frequency excitation pulse, G_z, MR gradient along the slice direction, G_y, MR gradient along the phase encoding direction, G_x, MR gradient along the readout directions, and ADC, analog to digital convert

Out-of-plane moments experience only non-selective RF excitations and do not experience slice-selective RF pulses. Therefore, the effective TR used for numerical simulations had to be adjusted accordingly for the different frequencies investigated. A single RF excitation required a TR of 3.15 ms for both slice-selective and non-selective RF pulses. As such, effective TR values of 12.6 (4 × 3.15), 22.5 (7 × 3.15), and 31.5 (10 × 3.15) ms were used to simulate 1 non-selective RF excitation applied after every third, sixth, and ninth slice-selective RF pulse, respectively. Flip angles ranging from 1° to 50° were evaluated during numerical simulations.

2.3 | In vitro phantom experiment: in-plane myocardial contrast

The T1MES phantom,[16] which contains 12 vials with different T_1 and T_2 values, was used to investigate the effect of flip angle on the myocardial contrast produced via the proposed method. The vial with a T_1 value of 354 ms was selected to represent the myocardial T_1 at peak contrast enhancement.[10] Myocardial contrast was calculated as the ratio of the mean signal intensity in the peak myocardial vial to the mean signal intensity in the 8 other vials with the following T_1 values: 415, 498, 515, 621, 724, 922, 943, and 1178 ms. These 8 vials were selected because they exhibited T_1 values representative of the range displayed by the myocardium during dynamic contrast enhancement (ie, between approximately 350 and 1050 ms).[10] The T_1 of phantom vials were previously measured using inversion recovery spin echo.[17]

For in vitro phantom experiments, SPGR with interleaved non-selective RF excitations (every third slice-select RF excitation) were acquired at the Nyquist sampling rate with the following pulse sequence parameters: radial k-space sampling with golden angle ordering (111.25°)[8] at 3 slices (0 mm slice gap), FOV = 288 × 288 mm^2, spatial resolution = 2.0 × 2.0 mm^2, slice thickness = 8 mm, acquisition matrix = 144 × 144, TE = 1.42 ms, and receiver bandwidth = 1085 Hz/pixel. Non-selective RF excitation was implemented by extending the slice thickness of slice-selective RF excitation to 500 mm. A truncated sinc pulse with 600 μs duration was used for both non-selective and slice-selective RF excitations. Measurements were repeated with flip angles ranging from 10° to 40° (the largest angle allowed by specific absorption rate [SAR] limitation) at increments of 5°. Manually drawn regions of interest were used to calculate the mean signal

intensity for different vials. Signal intensities were normalized with proton density images acquired with a flip angle of 5° (all other acquisition parameters were the same) to remove spatial variances because of coil sensitivities.

2.4 | In vivo study: patients

This study was approved by our local institutional review board (IRB) and was Health Insurance Portability and Accountability Act (HIPPA)-compliant. Written consent was obtained from all subjects. CMR scans were performed on a 3T system (MAGNETOM Vida, Siemens Healthcare, Erlangen, Germany) equipped with a gradient system capable of producing maximum gradient strength of 60 mT/m and maximum slew rate of 200 T/m/s. A body coil was used for radio-frequency excitation, and body surface and spine phased-array coils (around 30 elements) were used for signal reception.

Because of restrictions regarding the usage of gadolinium in healthy subjects, recruitment was limited to patients referred for a CMR exam with gadolinium. To avoid conflict with clinically required imaging sequences, no patients were referred for myocardial perfusion assessment. Considering these limitations, 22 patients (11 male, 60.2 ± 14.3 years) who were referred for myocardial viability assessment were prospectively recruited. Patient clinical history can be found in Supporting Information Table S1. Patients were divided into 2 groups and imaged with SPGR with or without interleaved non-selective RF excitations. Perfusion scans were performed at 3 slice locations (apex, mid, and base) using a bolus injection of 0.05 mmol/kg of gadobutrol with 10 mL of saline after contrast injection at a rate of 3 mL/s. Data acquisition started 10-20 s before the start of contrast injection and continued for ~2 min.

2.5 | In vivo study: acquisition and reconstruction

For in vivo studies, the same pulse sequence parameters as described for the in vitro phantom experiments were used, and SPGR without non-selective RF excitations was acquired with the optimal 30° flip angle.[10] GRAPPA Radial Gridding-Golden Angle Radial Parallel Imaging (GROG-GRASP)[18] with temporal finite difference sparsity and conjugated gradient descent optimization (36 iterations) was used to remove aliasing artifact from undersampled, ungated, free-breathing myocardial perfusion images acquired with (14 projections per frame, temporal resolution = 176.4 ms) and without (18 projections per frame, temporal resolution = 170.1 ms) interleaved non-selective RF (Supporting Information Figure S1). GROG-GRASP was used to enable fast GPU-based compressed sensing reconstruction of undersampled radial k-space data.[18] The number of radial projections per frame used for both SPGR pulse sequences were selected to achieve a similar temporal footprint of ~170 ms. Regularization weights of 0.0025 and 0.004 were used for SPGR with non-selective RF and SPGR without non-selective RF, respectively. For each acquisition type, an optimal regularization weight was empirically found by reconstructing 1 training data set with different regularization weights (range = 0.001 to 0.01; step size = 0.0005) and identifying the lowest weight that adequately removed aliasing artifacts while minimizing temporal blurring in the heart. Regularization weights were normalized with the maximum pixel intensity from the center 25% of time-averaged images. GROG-GRASP reconstruction was implemented in MATLAB (The MathWorks, Natick, MA). To reduce reconstruction time, principal component analysis was used to produce 8 virtual coils.

Reconstructed myocardial perfusion images were self-gated to diastole in the following order: a 72 × 72 region encompassing the heart was selected, and the energy within the cropped region was calculated for each temporal frame. MATLAB's built-in peak detection algorithm (findpeaks) was then used to isolate diastolic frames. Finally, the region around the heart was cropped manually, rather than automatically, as previously described.[19]

2.6 | Quantitative assessment of contrast-to-noise ratio

Contrast-to-noise ratio (CNR) was calculated for the mid slice of each perfusion data set as follows: (1) region-of-interests (ROIs) were drawn on the septum of the pre-contrast and peak-myocardial contrast phases; (2) noise ROI was drawn in the background of the of peak-myocardial contrast phases; (3) contrast was calculated by subtracting the mean signal found in pre-contrast and peak-myocardial contrast septal ROIs; and (4) CNR was calculated by dividing contrast by the standard deviation of the noise ROI. ROIs for all data sets were drawn by 1 reader (R.G.) using in-house MATLAB software. CNR for SPGR with and without non-selective RF were compared using an unpaired *t* test, where *P*-value <0.05 was deemed statistically significant.

2.7 | Qualitative visual assessment

The 22 sets of perfusion images were first interpolated 2-fold along the spatial dimension to a spatial resolution of 1.0 × 1.0 mm^2, then randomized and de-identified. Like previous studies,[20,21] the entire dynamic series for each perfusion data set (beginning with pre-contrast and extending beyond peak-myocardial contrast) for all 3 short-axis slices were evaluated

by 1 expert reader (S.K.) on a 5-point Likert scale. Myocardial perfusion was scored for conspicuity of wall enhancement (1 = nondiagnostic; 2 = poor; 3 = clinically acceptable; 4 = good; 5 = excellent), inflow/motion artifact level (1 = nondiagnostic; 2 = severe; 3 = moderate; 4 = mild; 5 = minimal), and streaking artifact level (1 = nondiagnostic; 2 = severe; 3 = moderate; 4 = mild; 5 = minimal). Scores for SPGR with and without non-selective RF were compared using the Wilcoxon rank-sum test. *P*-value <0.05 was deemed statistically significant.

3 | RESULT

A 30° flip angle and a frequency of 1 non-selective RF pulse after every 3 slice-selective RF pulses were deemed optimal for the proposed free-running SPGR acquisition. These choices were based on the following empirical observations; (1) numerical simulations revealed that higher frequencies (ie, every third slice-selective RF pulse) improved longitudinal signal suppression of out-of-plane moments. This improvement was especially noticeable for T_1 values corresponding to peak myocardium (T_1 ≥350 ms) and peak blood (T_1 ≥20 ms) for flip angles between 30° and 50° (Figure 2, red box); (2) the chosen flip angle and frequency yielded near-optimal myocardial contrast for all T_1-value combinations investigated during in vitro phantom experiments (Figure 3, red box); (3) in vitro experiments showed that the chosen flip angle and frequency produced myocardial contrast differences within ±0.05 for all slices acquired (Figure 3, blue box); (4) a 30° flip angle was found to consistently avoid the hardware's SAR-limit for the RF duration (600 μs), RF shape (truncated sinc), and TR (3.15 ms) used during in vivo scanning; and (5) the relatively high 30° flip angle can quickly drive out-of-plane spins entering the imaging plane to steady-state and, in doing so, further mitigates in-flow and motion artifacts. Figure 4 shows data collected in 2 patients who underwent free-running SPGR with or without interleaved non-selective RF. These images demonstrate the ability of additional non-selective RF pulses to eliminate magnetization loss because

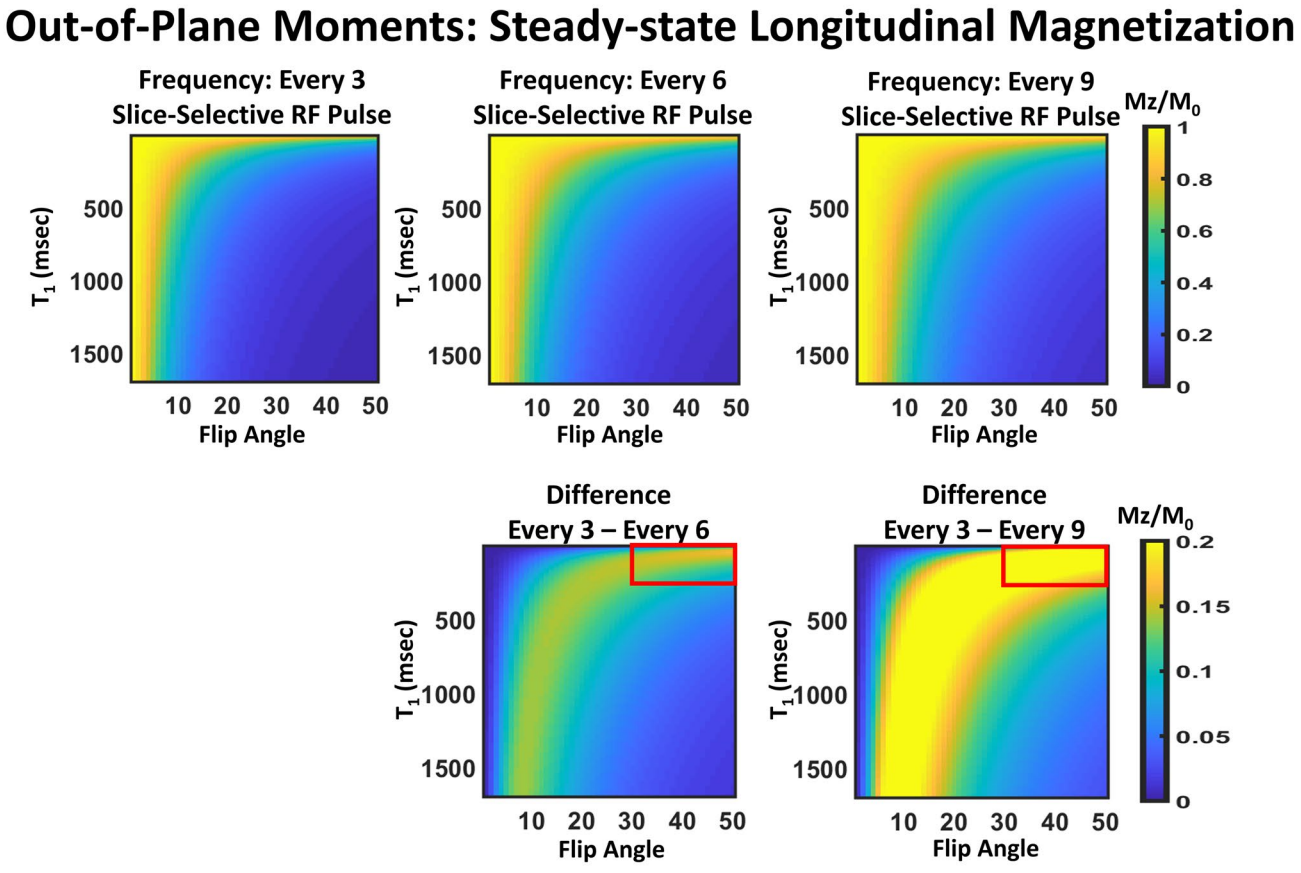

FIGURE 2 Bloch simulations exploring the effect of interleaved non-selective RF excitation frequency and flip angle on the normalized longitudinal signal intensity (M_z/M_0) of out-of-plane moments for T_1 values ranging from 1 to 1700 ms. Higher flip angles resulted in increased signal suppression for out-of-plane moments for all 3 non-selective RF excitation frequencies evaluated (ie, every 3rd, 6th, and 9th slice-selective RF pulse). Difference maps comparing non-selective RF excitation frequencies (ie, every 3rd to every 6th, and every 3rd to every 9th) show that higher frequencies (ie, every 3rd slice-selective RF excitation) improved signal intensity suppression for T_1 values associated with peak myocardium (T_1 ≥350 ms) and peak blood (T_1 ≥20 ms) contrast for flip angles between 30° and 50° (red box). These results suggest that high flip angles combined with high non-selective RF excitation frequencies provides superior magnetization suppression for out-of-plane moments

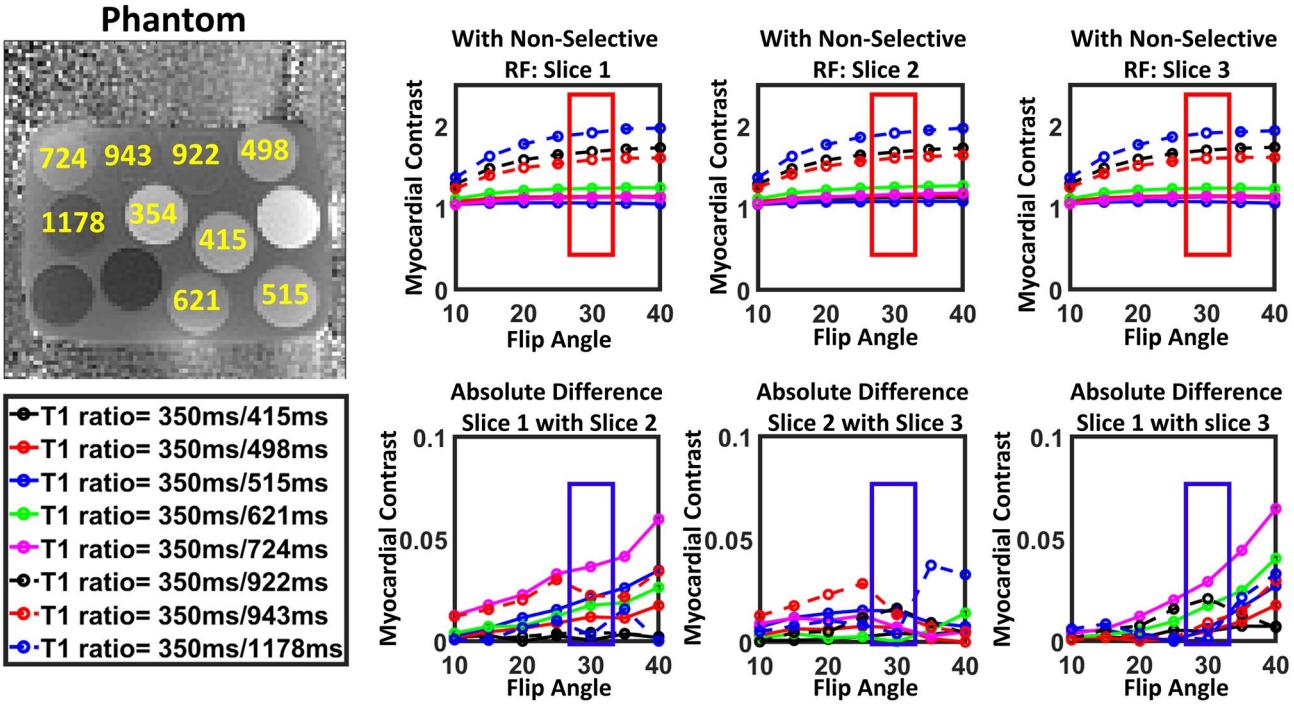

FIGURE 3 In vitro phantom experiments evaluating myocardial contrast of in-plane moments imaged using free-running SPGR with interleaved non-selective RF excitations. Myocardial contrast was defined as the ratio of the peak myocardium T_1 (354.0 ms) to other longer T_1 values (between 415-1178 ms) displayed by the myocardium during dynamic contrast enhancement. Interleaved non-selective RF excitations applied with a 30° flip angle were found to produce a near-optimal myocardial contrast for all T_1 ratios investigated (red box). A flip angle of 30° was also found to produce an absolute difference of less than 0.05 for quantified myocardial contrast across all 3 acquired slices (blue box)

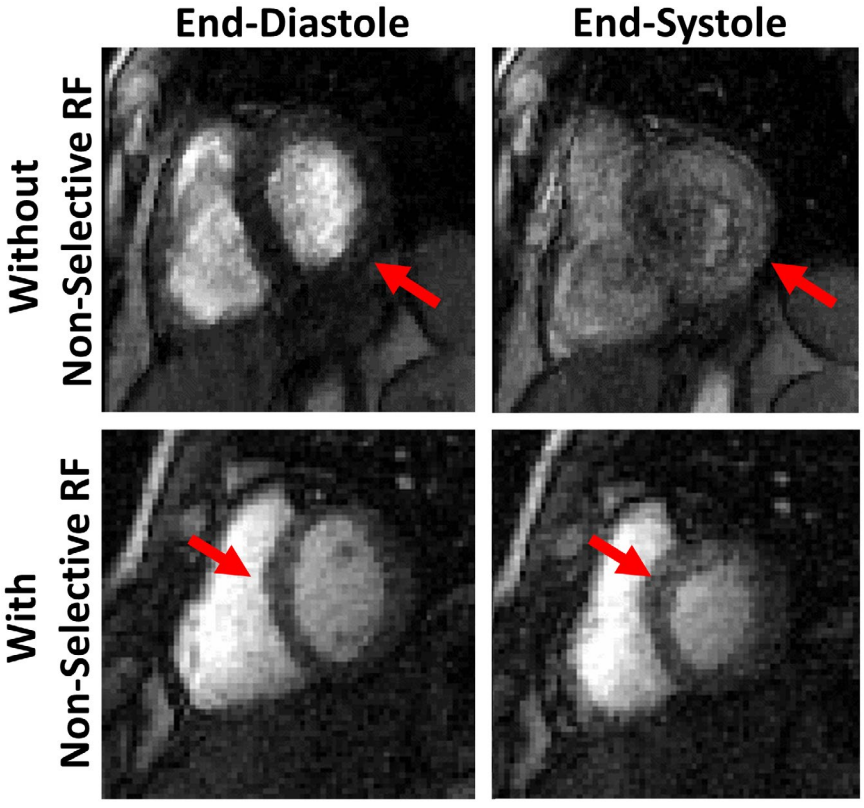

FIGURE 4 Ungated, free-breathing myocardial perfusion images for 2 patients imaged without (top) or with (bottom) interleaved non-selective RF excitations. For both patients, end-diastolic and end-systolic phases during the same heartbeat are shown to demonstrate motion-induced "flash" artifact. The addition of interleaved non-selective RF excitation produced T_1-weighted imaging, which showed greater resistance to motion artifacts (red arrow)

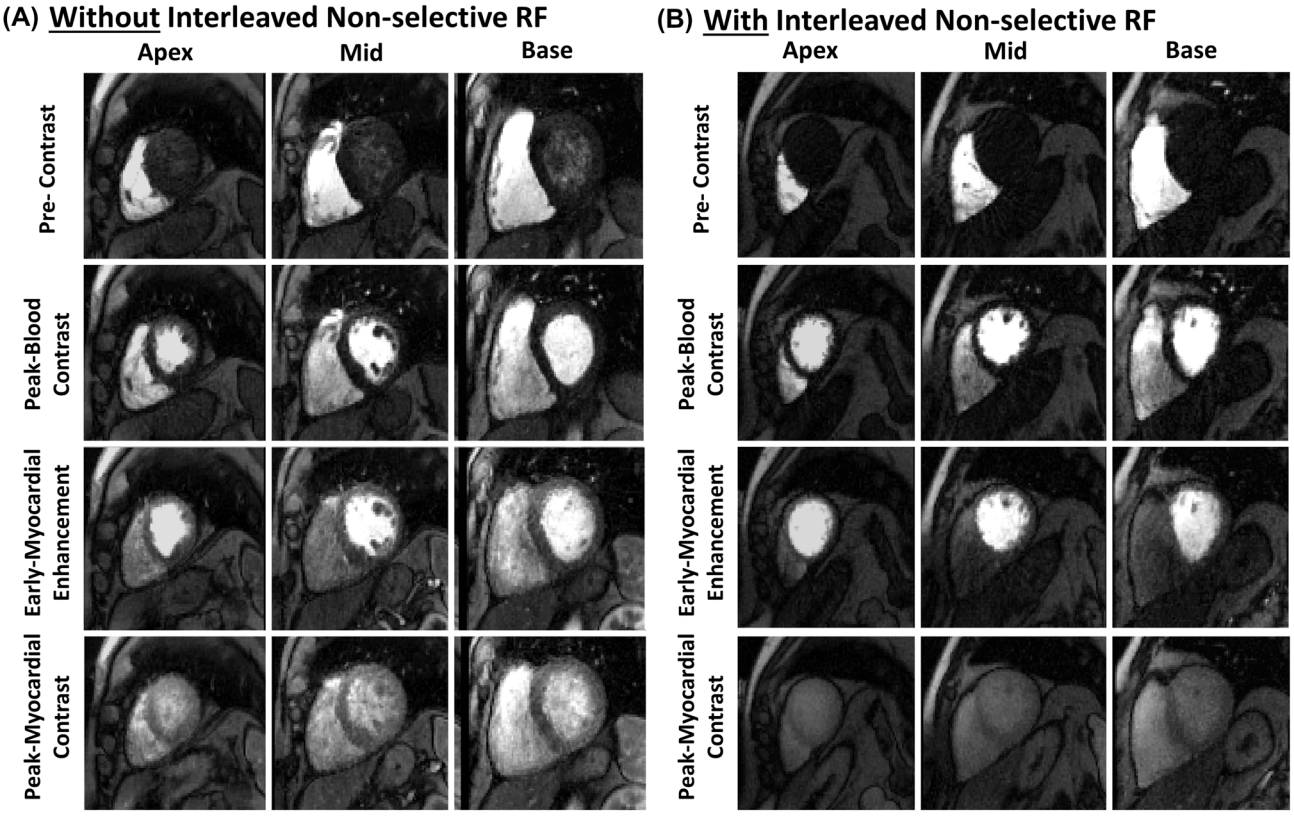

FIGURE 5 Representative diastolic myocardial perfusion images acquired using ungated, free-breathing, 2D multi-slice SPGR without (A) and with (B) interleaved non-selective RF excitations for 2 patients. Patients imaged using SPGR with and without non-selective RF excitations displayed an ejection fraction of 49% and 56%, respectively. For dynamic display, see Supporting Information Videos S1 and S2

of cardiac motion (red arrow). Representative ungated free-breathing myocardial perfusion images acquired using SPGR with and without non-selective RF at 4 contrast enhancement phases (pre-contrast, peak-blood contrast, early myocardium contrast, and peak-myocardium contrast) are shown in Figure 5. End-systolic and end-diastolic cardiac phases at 4 contrast enhancement phases are shown for SPGR without and with non-selective RF in Supporting Information Figures S2 and S3, respectively. Supporting Information Table S2 presents expert reader scores for ungated, free-breathing SPGR acquisitions with and without interleaved non-selective RF excitations. The addition of interleaved non-selective RF excitations significantly improved conspicuity of wall enhancement (mean score = 4.4 vs. 3.2, $P < .01$), inflow/motion artifact levels (average score = 4.5 vs. 2.5, $P < .01$), and streaking artifact levels (average score = 3.9 vs. 2.4, $P < .01$) for myocardial perfusion imaging. Interleaved non-selective RF excitations did not significantly alter CNR (mean score = 14.0 ± 5.1 vs. 15.9 ± 5.5, $P = .41$).

4 | DISCUSSION

In this study, inflow and motion artifacts in free-breathing, free-running CMR perfusion sequence were suppressed by interleaving non-selective RF excitations between slice-selective RF excitations during SPGR imaging with radial sampling. Numeric simulations and phantom experiments showed that a non-selective RF excitation with a flip angle of 30° applied after every third slice-selective RF excitation produced superior out-of-plane moment signal suppression. During in vivo experiments, the addition of interleaved non-selective RF reduced inflow/motion and streaking artifacts, improved myocardial enhancement conspicuity, and maintained CNR during free-running SPGR imaging.

Previous studies have shown that free-running SPGR can provide multi-slice ungated myocardial perfusion imaging.[9-11] Although promising, free-running SPGR presents with image artifacts resulting from the inflow of unsaturated spins into the imaging slice because of cardiac and respiratory motion and blood flow.[9,10] Both Judd et al[14] and Sharif et al[15] suggested using non-selective RF pulses during 2D multi-slice SPGR-based perfusion imaging. This strategy can suppress inflow and motion artifacts by driving the magnetization of the entire imaging volume to steady-state. The proposed approach is very similar to these 2 studies with important distinctions. Unlike Judd et al's[14] approach of acquiring 1 short-axis slice every 3 heartbeats, the proposed sequence mimicked Sharif et al's[15] example of acquiring all 3 short-axis slices in an interleaved

manner. Whereas Judd et al's[14] approach applied 60 non-selective RF excitations during magnetization preparation; the proposed sequence followed Sharif et al's[15] approach of applying interleaved non-selective RF excitations continuously throughout free-running SPGR. Unlike either Judd et al[14] or Sharif et al,[15] the proposed sequence was evaluated during free-breathing. Additionally, a 30° flip angle was used for non-selective RF excitations because in vitro phantom experiments showed that this flip angle produced near-optimal myocardial contrast within the SAR limit. Improvements provided by the proposed solution were confirmed by comparing free-breathing, ungated, myocardial perfusion acquired using SPGR with and without interleaved non-selective RF excitations in patients.

The present study has several limitations. Because of restrictions regarding usage of gadolinium in healthy subjects, the proposed sequence was not compared to conventional clinical perfusion imaging in healthy volunteers under rest and stress conditions. Numeric simulations did not account for heart rate and respiratory motion changes during free-breathing exams, but rather, explored the worst-case scenario in which fully unsaturated spins entered the imaging plane because of inflow or motion. The non-selective RF excitations reduced image acquisition efficiency and slightly decreased temporal resolution (170 vs. 176 ms). Only 3 slices were acquired during myocardial perfusion imaging. Additional studies are required to explore increasing slice coverage through simultaneous multi-slice[12,13] and 3-dimensional myocardial perfusion[11,22-25] imaging. Myocardial blood flow (MBF) was not quantified for both free-running SPGR with and without non-selective RF. Future studies are needed to explore MBF quantification using the proposed free-running SPGR. An alternative strategy for suppressing in-flow and motion artifacts in free-running SPGR is to filter high-frequency components corresponding to inflow and motion, and studies exploring such a strategy are warranted. Residual streaking artifacts, which reduced image quality, were observed for both SPGR with and without non-selective RF. Observed streaking artifacts may have resulted from reduced reconstruction performance because of breathing motion-induced loss of temporal redundancy. RF duration or excitation shape was not optimized for interleaved non-selective RF pulses. Instead, slice-selective RF was altered to mimic a "hard pulse" by adjusting the slice-select gradient profile to enable volumetric excitation. The same acquisition flip angle was used for both slice-selective and non-selective excitations during free-running SPGR acquisition; moreover, different RF excitation flip angles would have resulted in oscillatory behavior in steady-state longitudinal magnetization across the readout. T_2^* effects were not accounted for during Bloch simulations, because TE << T_2 typically holds true for first pass myocardial perfusion.[10] During qualitative assessment, artifact scores integrated information along the entire dynamic series and, as such, did not reflect artifacts found in individual time frames.

In this study, the capacity for rest and stress free-running CMR perfusion imaging to detect myocardial perfusion defects was not assessed. Hence, additional studies are needed to compare the diagnostic accuracy of the proposed SPGR pulse sequence to conventional myocardial perfusion CMR with saturation preparation using well-established invasive measurements such as FFR. However, the proposed sequence's temporal resolution (~170 ms) is significantly lower than that needed for near end-systolic imaging and that is achievable for standard perfusion imaging (<100 ms).[7] This is a major limitation because the streaking artifact level in the myocardium is expected to increase during stress because of elevated heart rates.[9] There is further need for technical innovations to make the proposed sequence robust before conducting such studies.

In conclusion, this study evaluated the capacity of non-selective RF excitations interleaved between slice-selective excitations to reduce inflow and motion artifacts during free-breathing, free-running SPGR-based myocardial perfusion. Further studies are warranted to assess the impact of adding non-selective RF excitations to free-running myocardial perfusion on diagnostic accuracy.

ACKNOWLEDGMENTS

Dr. Nezafat is funding by the NIH (5R01HL127015-02, 1R01HL129157-01A1, 5R01HL129185, and 1R01HL154744) and the American Heart Association (15EIA22710040). Dr. Haji-Valizadeh is supported by the NIH (5T32HL007374-41).

CONFLICT OF INTEREST

Dr. Cai is an employee of Siemens Medical Solutions USA, Inc. and works as an on-site research scientist at BIDMC. Dr. Nezafat has a research agreement with Siemens Medical Solutions USA, Inc. Dr. Haji-Valizadeh is currently an employee of Canon Medical Research USA Inc. The work presented in this study was performed during his post-doctoral training fellowship at Beth Israel Deaconess Medical Center.

DATA AVAILABILITY STATEMENT

Codes used for Bloch simulations and multi-T_1 phantom data set analysis are openly available on Harvard dataverse (https://dataverse.harvard.edu/dataverse/cardiacmr), reference number doi.org/10.7910/DVN/SKDEYZ.

ORCID

Hassan Haji-Valizadeh https://orcid.org/0000-0002-7652-1748
Rui Guo https://orcid.org/0000-0002-5188-6281
Selcuk Kucukseymen https://orcid.org/0000-0002-9757-3088

REFERENCES

1. Jahnke C, Nagel E, Gebker R, et al. Prognostic value of cardiac magnetic resonance stress tests: adenosine stress perfusion and dobutamine stress wall motion imaging. *Circulation*. 2007;115:1769-1776.
2. Korosoglou G, Elhmidi Y, Steen H, et al. Prognostic value of high-dose dobutamine stress magnetic resonance imaging in 1,493 consecutive patients: assessment of myocardial wall motion and perfusion. *J Am Coll Cardiol*. 2010;56:1225-1234.
3. Vasu S, Bandettini WP, Hsu L-Y, et al. Regadenoson and adenosine are equivalent vasodilators and are superior than dipyridamole- a study of first pass quantitative perfusion cardiovascular magnetic resonance. *J Cardiovasc Magn Reson*. 2013;15:85.
4. Raman SV, Dickerson JA, Jekic M, et al. Real-time cine and myocardial perfusion with treadmill exercise stress cardiovascular magnetic resonance in patients referred for stress SPECT. *J Cardiovasc Magn Reson*. 2010;12:41.
5. Greenwood JP, Maredia N, Younger JF, et al. Cardiovascular magnetic resonance and single-photon emission computed tomography for diagnosis of coronary heart disease (CE-MARC): a prospective trial. *Lancet*. 2012;379:453-460.
6. Nagel E, Greenwood JP, McCann GP, et al. Magnetic resonance perfusion or fractional flow reserve in coronary disease. *N Engl J Med*. 2019;380:2418-2428.
7. Kellman P, Hansen MS, Nielles-Vallespin S, et al. Myocardial perfusion cardiovascular magnetic resonance: optimized dual sequence and reconstruction for quantification. *J Cardiovasc Magn Reson*. 2017;19:43.
8. Winkelmann S, Schaeffter T, Koehler T, Eggers H, Doessel O. An optimal radial profile order based on the Golden Ratio for time-resolved MRI. *IEEE Trans Med Imaging*. 2007;26:68-76.
9. Sharif B, Dharmakumar R, Arsanjani R, et al. Non-ECG-gated myocardial perfusion MRI using continuous magnetization-driven radial sampling. *Magn Reson Med*. 2014;72:1620-1628.
10. Sharif B, Arsanjani R, Dharmakumar R, Bairey Merz CN, Berman DS, Li D. All-systolic non-ECG-gated myocardial perfusion MRI: feasibility of multi-slice continuous first-pass imaging. *Magn Reson Med*. 2015;74:1661-1674.
11. DiBella EV, Chen L, Schabel MC, Adluru G, McGann CJ. Myocardial perfusion acquisition without magnetization preparation or gating. *Magn Reson Med*. 2012;67:609-613.
12. Wang H, DiBella EVR, Adluru G, Park DJ, Taylor MI, Bangerter NK. Effect of slice excitation profile on ungated steady state cardiac perfusion imaging. *Biomed Phys Eng Express*. 2017;3:027001.
13. Tian YE, Mendes J, Wilson B, et al. Whole-heart, ungated, free-breathing, cardiac-phase-resolved myocardial perfusion MRI by using continuous radial interleaved simultaneous multi-slice acquisitions at sPoiled steady-state (CRIMP). *Magn Reson Med*. 2020;84:3071-3087.
14. Judd RM, Reeder SB, Atalar E, McVeigh ER, Zerhouni EA. A magnetization-driven gradient echo pulse sequence for the study of myocardial perfusion. *Magn Reson Med*. 1995;34:276-282.
15. Sharif B, Dharmakumar R, Berman DS, Li D, Merz NB. End-systolic myocardial perfusion MRI using a hybrid 2D/3D steady-state acquisition scheme: towards reliable detection of subendocardial ischemia in coronary microvascular dysfunction. Paper presented at: Proceedings of the 24nd Annual Meeting of ISMRM. 2016. p. 467.
16. Captur G, Gatehouse P, Keenan KE, et al. A medical device-grade T1 and ECV phantom for global T1 mapping quality assurance-the T1 mapping and ECV standardization in cardiovascular magnetic resonance (T1MES) program. *J Cardiovasc Magn Reson*. 2016;18:58.
17. Moon JC, Messroghli DR, Kellman P, et al. Myocardial T1 mapping and extracellular volume quantification: a society for cardiovascular magnetic resonance (SCMR) and CMR working group of the European Society of Cardiology consensus statement. *J Cardiovasc Magn Reson*. 2013;15:92.
18. Benkert T, Tian Y, Huang C, DiBella EVR, Chandarana H, Feng L. Optimization and validation of accelerated golden-angle radial sparse MRI reconstruction with self-calibrating GRAPPA operator gridding. *Magn Reson Med*. 2018;80:286-293.
19. Harrison A, Adluru G, Damal K, et al. Rapid ungated myocardial perfusion cardiovascular magnetic resonance: preliminary diagnostic accuracy. *J Cardiovasc Magn Reson*. 2013;15:26.
20. Naresh NK, Haji-Valizadeh H, Aouad PJ, et al. Accelerated, first-pass cardiac perfusion pulse sequence with radial k-space sampling, compressed sensing, and k-space weighted image contrast reconstruction tailored for visual analysis and quantification of myocardial blood flow. *Magn Reson Med*. 2019;81:2632-2643.
21. Fan L, Shen D, Haji-Valizadeh H, et al. Rapid dealiasing of undersampled, non-Cartesian cardiac perfusion images using U-net. *NMR Biomed*. 2020;33:e4239.
22. Mendes JK, Adluru G, Likhite D, et al. Quantitative 3D myocardial perfusion with an efficient arterial input function. *Magn Reson Med*. 2020;83:1949-1963.
23. Giri S, Xue H, Maiseyeu A, et al. Steady-state first-pass perfusion (SSFPP): a new approach to 3D first-pass myocardial perfusion imaging. *Magn Reson Med*. 2014;71:133-144.
24. Shin T, Hu HH, Pohost GM, Nayak KS. Three dimensional first-pass myocardial perfusion imaging at 3T: feasibility study. *J Cardiovasc Magn Reson*. 2008;10:57.
25. Akçakaya M, Basha TA, Pflugi S, et al. Localized spatio-temporal constraints for accelerated CMR perfusion. *Magn Reson Med*. 2014;72:629-639.

SUPPORTING INFORMATION

Additional Supporting Information may be found online in the Supporting Information section.

FIGURE S1 GROG-GRASP reconstruction used for ungated myocardial perfusion imaging. During pre-processing, GROG was used to translate radial polar k-space data onto a Cartesian grid to produce both time-averaged, multi-coil images and time-resolved, multi-coil perfusion k-space data (purple boxes). Time-resolved, multi-coil perfusion k-space was produced by gridding 14 projections per frame for SPGR with interleaved non-selective RF and 18 projections per frame for SPGR without interleaved non-selective RF. Time averaged, multi-coil images were used to derive auto-calibrated coil sensitivity profiles (blue box), which were subsequently inputted with density-compensated (green box), time-resolved, multi-coil perfusion k-space data into a SENSE (sensitivity encoding) operator to produce coil-combined, time resolved, undersampled perfusion images (red boxes). Iterative nonlinear conjugate gradient optimization was used to remove aliasing artifact from coil-combined, time resolved, undersampled perfusion images

FIGURE S2 End-systolic and end-diastolic cardiac phases for SPGR without non-selective RF acquired at pre-contrast (A), peak-blood contrast (B), early-myocardial (C), and peak-myocardial (D), enhancement phases. For dynamic display, see Supporting Information Videos S1 and S3

FIGURE S3 End-systolic and end-diastolic cardiac phases for SPGR with non-selective RF acquired at pre-contrast (A), peak-blood contrast (B), early myocardial (C), and peak-myocardial (D) enhancement phases. For dynamic display, see Supporting Information Videos S2 and S4

TABLE S1 Clinical history summary for patients enrolled in study

TABLE S2 Summary of expert reader scores for ungated myocardial perfusion imaging obtained with 2D multi-slice SPGR acquisitions with and without interleaved non-selective RF excitations. Reported values represent mean (range min:max)

VIDEO S1 Movie display of the end-diastolic myocardial perfusion phases acquired with free-running SPGR without non-selective RF shown in Figure 5A and Supporting Information Figure S2

VIDEO S2 Movie display of the end-diastolic myocardial perfusion phases acquired with free-running SPGR with non-selective RF shown in Figure 5B and Supporting Information Figure S3

VIDEO S3 Movie display of the end-systolic myocardial perfusion phases acquired with free-running SPGR without non-selective RF shown in Supporting Information Figure S2

VIDEO S4 Movie display of the end-systolic myocardial perfusion phases acquired with free-running SPGR with non-selective RF shown in Supporting Information Figure S3

How to cite this article: Haji-Valizadeh H, Guo R, Kucukseymen S, et al. Artifact reduction in free-breathing, free-running myocardial perfusion imaging with interleaved non-selective RF excitations. *Magn Reson Med*. 2021;86:954–963. https://doi.org/10.1002/mrm.28765